Pol. J. Environ. Stud. Vol. XX, No. X (XXXX), 1-15

DOI: *10.15244/pjoes/222417* ONLINE PUBLICATION DATE: 2026-09-17

Original Research

Unraveling the Land-Water-Ecology Nexus and Water-Ecological Function Mismatch: Drivers of Aquatic Ecosystem Integrity in the Yellow River Basin

Xiao Feng[1]*, Xigan Sun[2], Huibo Hao[1]

[1]School of Economics and Management, Ningxia University, 489 Helan Mountain West Road, Xixia District, Yinchuan 750021, China

[2]School of Agriculture, Ningxia University, 489 Helan Mountain West Road, Xixia District, Yinchuan 750021, China

Received: 03 April 2026

Accepted: 25 May 2026

Abstract

In the water-stressed Yellow River Basin (YRB), land-use intensification (LUI) severely threatens water-related ecosystem services (WRES) critical for regional aquatic integrity. This study evaluates the spatiotemporal patterns and drivers of Habitat Quality (HQ, reflecting watershed regulation) and Biodiversity Conservation Function (BCF, indicating freshwater ecosystem health) from 2008 to 2023. Using the Integrated Valuation of Ecosystem Services and Trade-offs (InVEST) model, net primary productivity (NPP)-based assessment, Standard Deviational Ellipse (SDE), and in combination with eXtreme Gradient Boosting (XGBoost) and Shapley Additive Explanation (SHAP) analysis, we found that (1) while HQ remained stable (0.68-0.70), BCF exhibited a "southeast high, northwest low" gradient, (2) NPP, temperature, and precipitation are the primary natural drivers, and (3) a significant "water-ecological function mismatch" exists in the middle S-shaped bend due to water scarcity. The findings provide a scientific basis for prioritizing ecological compensation and balancing land pressure with aquatic conservation in arid and semi-arid regions.

Keywords: Yellow River Basin (YRB), water-related ecosystem services (WRES), land-use intensification (LUI), eXtreme Gradient Boosting (XGBoost), water-ecological function mismatch

Introduction

The YRB is a vital ecological corridor and water source, yet its integrity is increasingly compromised by LUI [1-4]. While LUI drives socioeconomic growth, it alters hydrological regimes [5-7], degrading two pillars of WRES: HQ and BCF. HQ is not only a prerequisite for biodiversity but also forms the basis for ecosystem service provision, including water purification, flow regulation, and sediment retention [8-10]. BCF reflects the capacity of an ecosystem to maintain genetic, species, and ecosystem diversity [11, 12], which is fundamental for freshwater ecosystem stability and resilience [13, 14]. Despite their importance,

*e-mail: fx2010@nxu.edu.cn

0009-0002-0321-7574

the integrated spatiotemporal relationship between LUI and these services remains insufficiently explored.

To fill this gap, this study utilizes the InVEST model [15-17] and NPP-quantitative evaluation to analyze HQ and BCF dynamics from 2008 to 2023 [18-20]. By incorporating SDE spatial analysis and an interpretable XGBoost-SHAP framework, we aim to: (1) analyze how LUI influences the spatiotemporal patterns of WRES, specifically HQ and BCF; (2) identify the key drivers, with a focus on hydro-climatic factors, shaping these patterns using interpretable machine learning; and (3) provide insights for integrated watershed management that harmonizes land-use planning with the conservation of aquatic ecosystems and sustainable water resource utilization.

Materials and Methods

Research Area Overview

Fig. 1 shows the geographical scope and land use types in the YRB. The YRB originates from the Qinghai-Tibet Plateau, which lies between 32°-42°N and 96°-119°E [21]. It passes through nine provinces and autonomous territories as it flows eastward: Inner Mongolia, Qinghai, Gansu, Ningxia, Shaanxi, Shanxi, Sichuan, Henan, and Shandong. The drainage basin is 5,464 km long and covers 790,000 km^2 [22].

Encompassing China's three major topographic terraces, the YRB has an average annual rainfall of approximately 473.99 mm [23], with significant spatial climatic variability. The west is dry, and the east is humid, due to air circulation and monsoons. The upper sections of the Yellow River traverse the Qinghai-Tibet Plateau, a region abundant in hydropower resources and an essential water source [24]. The middle reaches traverse the Loess Plateau and the Hanzhong Plain, where significant soil erosion occurs. The lower reaches are home to vast wetland ecosystems rich in biological diversity [25]. With a land area of 19%, the YRB is the second largest river system in China [26]. As a crucial water source region and ecological functional area, it is an important strategic zone for China's high-quality growth and ecological conservation [27]. Its ecological functions are of great importance for the establishment of China's ecological civilization and high-quality development of arid and semi-arid regions [28, 29]. China published the "Ecological Conservation and High-Quality Development Plan for the Yellow River Basin" in 2021, establishing systematic governance and development to promote coexistence among the environment, population, and resources within the basin. The basis and prerequisite for both conservation and superior economic development is ecology [30]. Positive results have been obtained from long-term ecological governance and construction; nonetheless, enduring issues like water shortage, ecological fragility, soil erosion, and competition for land resources in the context of socioeconomic development along the river still exist [31]. Simultaneously, the growing demand for ecological advantages necessitates the improvement of

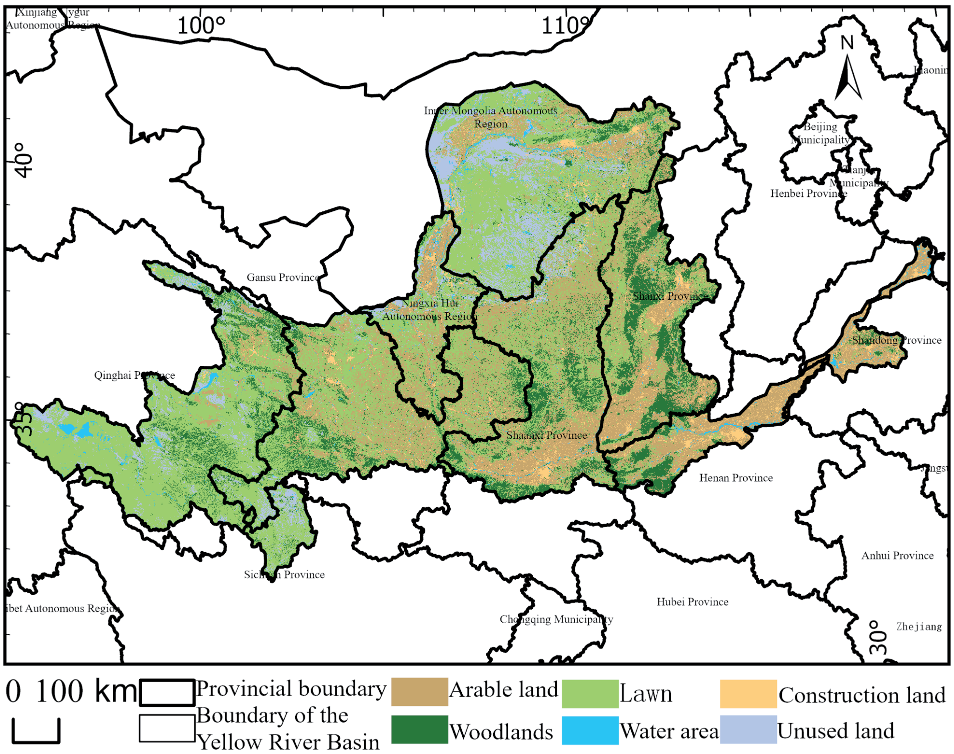

Fig. 1. Geographic location and land use types in the YRB.

ecological services and infrastructure to ensure high-quality growth [32, 33]. The main factor influencing changes in ecosystem service values is LUI [34-36]. Discovering how LUI in the YRB is changing in relation to its water-related ecosystem service values and aquatic biodiversity conservation function has critical implications for watershed ecological security and sustainable water resource management. This study offers valuable insights for enhancing freshwater biodiversity, realizing the value of WRES, and guiding basin-wide land use planning that prioritizes hydrological process protection.

Data Sources and Processing

To demonstrate the connection between HQ, WRES, and BCF within the YRB, this study employs the basin as its research unit. It integrates natural and socioeconomic demographic data, such as elevation, NPP, and LUI. Landsat TM remote sensing imagery from 2008-2023 is used to evaluate land use data; additional data sources are provided in Table 1. ArcGIS 10.8 software was used to resample and project all the data, resulting in a single spatial resolution of 1 km × 1 km in the WGS_1984_Albers coordinate system.

Research Methods

HQ Assessment – Invest Model

By evaluating HQ using LUI as a basis [37], the InVEST model assesses HQ based on LUI patterns [38-40]. It can reflect varying degrees of HQ and biodiversity abundance. The method is based on regional land use patterns and integrates the relative impact of each biodiversity threat, the relative sensitivity of different habitat types to threats, and the distance between habitat grids and threat sources. This method determines each landscape's suitability, the sensitivity to various hazards, and the distance and weight of threat sources. The research area's HQ index is then determined, and an HQ map is produced. Thus, among regional land use types, HQ is a dimensionless function of habitat appropriateness and habitat degradation degree [41, 42]. The habitat degradation level represents the degree of degradation caused by habitat danger factors, which are as follows:

$$Q_{xj} = H_j\left[1 - \frac{D_{xj}^z}{D_{xj}^z + k^z}\right] \quad (1)$$

$$D_{xj} = \sum_{r=1}^{R}\sum_{y=1}^{Y_r}\left(\frac{\omega_r}{\sum_{r=1}^{R}\omega_r}\right) r_y i_{rxy} \beta_x S_{jr} \quad (2)$$

$$i_{rxy} = 1 - \frac{d_{xy}}{d_{rmax}} \quad (3)$$

Here, r stands for the habitat's threat source, y for the grid cell inside threat source r, ω_r for the r-th threat source's weight, r_y for the r-th threat source's intensity inside grid cell y, i_{rxy} for the r-th threat source's influence attenuation function on grid cell x within grid cell y, and β_x for the accessibility of grid cell x. S_{jr} indicates how sensitive land use j is to threat source r, d_{ry} is the separation between grid cell x (habitat) and grid cell y (threat source), and d_{rmax} is the threat source r's maximum influence range.

The study region identified agriculture, urban land, rural residential land, industrial/mining and transportation land, and unutilized land as threat factors based on pertinent research and the Yellow River's actual conditions [43, 44]. They were identified by their spatial decay types, weights, and maximum influence distances. Parameters, including habitat suitability and

Table 1. Data sources and description.

Data Type	Data Source	Data resolution
Boundaries of the Yellow River Basin and China's Administrative Divisions	https://www.resdc.cn/ (CAS)	Vector data
Net Primary Productivity (NPP)	https://www.resdc.cn/ (CAS)	1 km*1 km
Elevation	https://www.resdc.cn/ (CAS)	1 km*1 km
Slope	Calculated from elevation data	1 km*1 km
Precipitation	National Earth System Science Data Center (https://www.geodata.cn/)	1 km*1 km
Air temperature	National Earth System Science Data Center (https://www.geodata.cn/)	1 km*1 km
NDVI	National Earth System Science Data Center (https://www.geodata.cn/)	1 km*1 km
Population density	World pop website (http://www.worldpop.org/)	1 km*1 km
Regional Gross Domestic Product	Data Center for Resource and Environmental Science, Chinese Academy of Sciences (http://www.resdc.cn)	1 km*1 km
Road	OSM website https://www.openstreetmap.org /	1 km*1 km

susceptibility to threat variables, were then determined (Fig. 2 and Fig. 3). The HQ of the YRB was assessed by extracting threat factor layers. (Table 2)

BCF Index

Following the technical guidelines for ecological protection redlines and building on studies by Zhang and Li [45, 46], this study employed an NPP quantitative method to assess the BCF [47-49]. This index is designed to reflect the capacity of an ecosystem to maintain freshwater biodiversity and ecological integrity, integrating variables central to the hydrological and ecological cycle:

$$S_b = NPP \times F_p \times F_t \times (1 - F_a) \quad (4)$$

Here, S_b denotes the BCF index, *NPP* represents net primary productivity of vegetation (linked to vegetation water use and carbon sequestration), F_p indicates annual precipitation (direct water input), F_t signifies annual mean temperature (regulating evapotranspiration and water balance), and F_a reflects the altitude factor. A higher BCF index indicates greater potential for sustaining aquatic biodiversity and associated WRES.

Standard Deviational Ellipse (SDE)

Lefever proposed the SDE in 1926 to analyze the directional features of spatial distribution. The element's

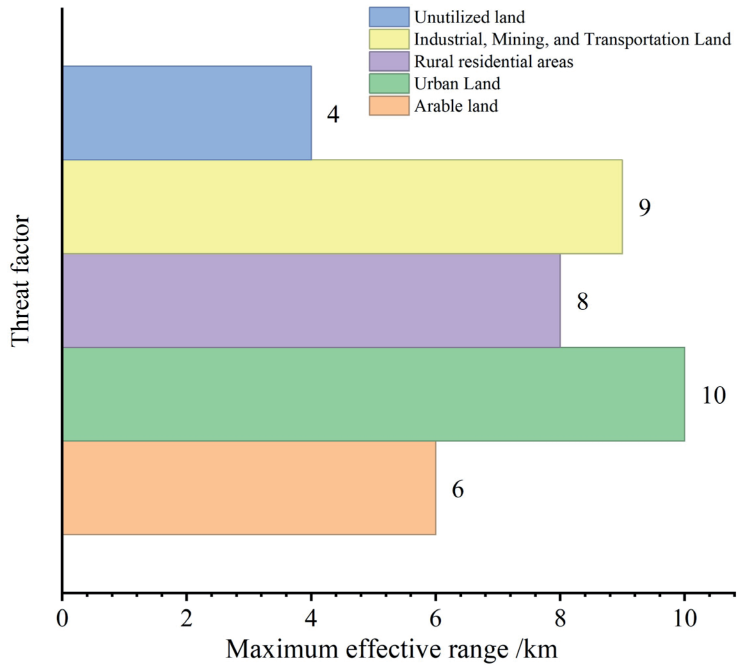

Fig. 2. Maximum effective range of threat factors.

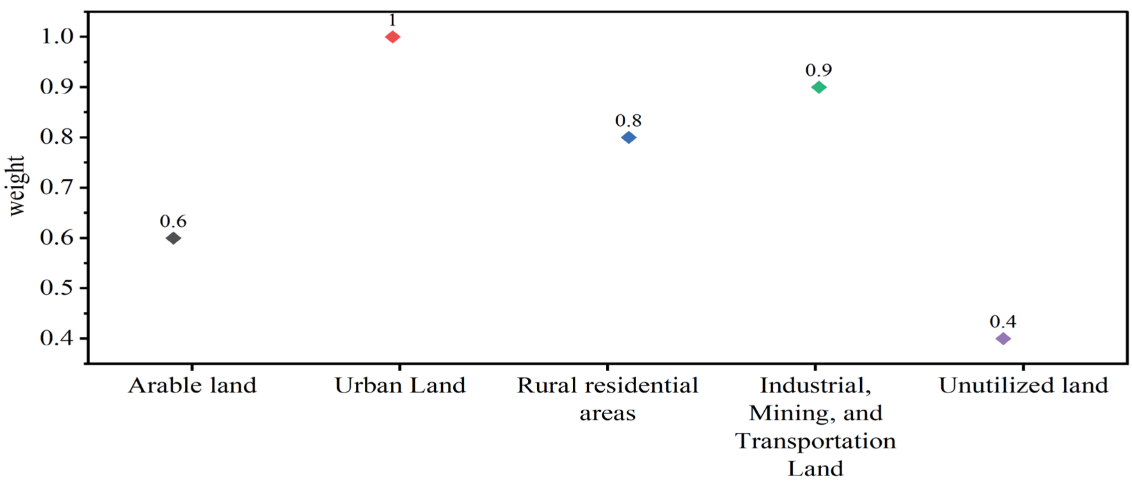

Fig. 3. Weight of threat factors.

Table 2. Threat factor attributes.

Threat factor	Maximum effective range /km	Weight	Decay Type
Arable land	6	0.6	Linear
Urban Land	10	1	Index
Rural residential areas	8	0.8	Index
Industrial, Mining, and Transportation Land	9	0.9	Index
Unutilized land	4	0.4	Linear

principal spatial distribution range is represented by the SDE's distribution range, and its mean center functions as the element's spatial distribution center of gravity [50, 51]. Important traits, including the aggregation center, evolutionary dynamics, and spatial orientation, are correlated with the ellipse's center position, area size, and rotation angle [52], respectively. To investigate the geographical evolution patterns of BCF in the YRB, the following methodology uses SDE:

$$\overline{X}_w = \frac{\sum_{i=1}^{n} w_i x_i}{\sum_{i=1}^{n} w_i} \quad \overline{Y}_w = \frac{\sum_{i=1}^{n} w_i y_i}{\sum_{i=1}^{n} w_i} \tag{5}$$

$$\tan\theta = \frac{\left(\sum_{i=1}^{n} w_i^2 \bar{x}_i^2 - \sum_{i=1}^{n} w_i^2 \bar{y}_i^2\right) + \sqrt{\left(\sum_{i=1}^{n} w_i^2 \bar{x}_i^2 - \sum_{i=1}^{n} w_i^2 \bar{y}_i^2\right)^2 + 4\sum_{i=1}^{n} w_i^2 \bar{x}_i^2 \bar{y}_i^2}}{2\sum_{i=1}^{n} w_i^2 \bar{x}_i^2 \bar{y}_i^2} \tag{6}$$

$$\sigma_x = \sqrt{\frac{\sum_{i=1}^{n}(w_i\bar{x}_i \cos\theta - w_i\bar{y}_i \sin\theta)^2}{\sum_{i=1}^{n} w_i^2}}, \quad \sigma_y = \sqrt{\frac{\sum_{i=1}^{n}(w_i\bar{x}_i \sin\theta - w_i\bar{y}_i \cos\theta)^2}{\sum_{i=1}^{n} w_i^2}} \tag{7}$$

$$S = \pi\sigma_x\sigma_y \tag{8}$$

Here, the centroid coordinates are represented by $\overline{X}$ w and $\overline{Y}$ w in Equations (5) to (8); the weight is represented by w_i; the elliptical azimuth is represented by θ; the coordinate deviations from the mean center for each study object are indicated by $\bar{x}_i$ and $\bar{y}_i$ respectively; the standard deviations along the x-axis and y-axis are indicated by σ_x and σ_y, respectively; and S is the elliptical area. This analysis reveals how the core spatial distribution of this water-linked ecosystem service has shifted in response to environmental and anthropogenic changes, providing insights into the evolving spatial relationship between ecological function and water resource availability.

Xgboost Machine Learning

Based on the gradient boosting architecture, XGBoost is a potent machine learning algorithm created especially to improve prediction accuracy [53]. It excels at handling large datasets, shows exceptional capabilities in regulating model complexity and reducing overfitting, and gradually builds a series of weak learners to improve model performance. This study uses the XGBoost model to accurately identify the intricate driving processes controlling the BCF in the YRB [54]. In particular:

$$\hat{y}_i = \Sigma_{n=1}^{N} f_n(x_i), f_n \subseteq H \tag{9}$$

Here, the expected value of BCF in the YRB is represented by the equation's $\hat{y}_i$. The feature vector of sample *i*, represented by x_i, includes various factors that affect the BCF. The predicted value of the *n*-th base learner for sample x_i is $f_n(x_i)$. The set of all potential base learners is represented by *H*, while the total number of base learners is represented by *N*.

The following objective function, which focuses on reducing model error while managing complexity, is optimized to accomplish model training:

$$T = \Sigma_{i=1}^{n} l(y_i, \hat{y}_i) + \Sigma_{i=1}^{N} \Omega(f_n) \tag{10}$$

Here, the error function in the equation, $l(y_i, \hat{y}_i)$, quantifies the difference between the expected value $\hat{y}_i$ and the actual coupling coordination degree y_i. The regularization term $\Omega(f_n)$ is intended to limit the base learner's complexity to avoid overfitting and improve the model's performance on unknown inputs.

Shapley Additive Explanation of the Xgboost Algorithm, Interpreted Using SHAP Values (Xgboost-SHAP Framework)

The precise direction and magnitude of each driver's influence on BCF cannot be intuitively explained by the XGBoost model. To understand the XGBoost model's black-box nature, the SHAP approach is presented. The Shapley value in game theory serves as an inspiration for SHAP, which evaluates the relative significance of individual characteristics in machine learning models. To determine the final effect value, weighted averaging is used to calculate the marginal contribution of each characteristic across various combinations [55]. Because it may be applied to both local and global explanations, this approach is a very interpretable research tool [56]. The formula for calculation is as follows:

$$\varphi_i = \Sigma_{S\subseteq H\{i\}}\left[\frac{|S|!\,(|H|-|S|-1)!}{|H|!}\right]\left(t(S\cup\{i\})-t(S)\right) \tag{11}$$

Here, the contribution of driving factor i to the final prediction is represented by the SHAP value, φ_i, in the formula. H is the total set of all features, S is a subset of H that does not include feature i, and $t(S)$ is the model prediction result for the combination of features in subset S.

Results and Discussion

Characteristics of HQ Changes in the YRB

To assess the spatial variation, HQ was categorized into five classes: very low (0.00-0.15), low (0.15-0.43), medium (0.43-0.70), high (0.70-0.89), and very high (0.89-1.00). This classification was performed using the natural breaks method in ArcGIS 10.8. For the analysis of LUI in the YRB spanning 2008-2023, the intermediate year 2018 served as the baseline for applying this classification scheme. The distribution is shown in Fig. 4.

The YRB maintained generally satisfactory HQ, with an average score consistently above 0.68 from 2008-2023. The trend showed fluctuations around a high baseline. While the share of lower-grade areas fell by 1.1 percentage points, the proportion of low-grade areas climbed progressively from 3.2% to 5.34%. There was a 1.76 percentage point increase in the percentage of medium-grade areas. While the percentage of high-grade areas fell from 47.67% to 43.53%, the area designated as a very high grade increased from 11.95% to 13.27%. The decline in high-grade areas was primarily concentrated in eastern Qinghai Province, near the source of the Yellow River, where water-ecological functional zone conservation efforts have produced notable outcomes.

The HQ exhibited a distinct "higher in the west, lower in the east" gradient. High-HQ clusters in the western headwaters are crucial for water conservation and retention, whereas low-HQ areas in the eastern plains correlate with intensive human activity and heightened risks to water quality. The Qinghai Province and the Qinghai-Sichuan border region contain most areas with high and moderately high HQ. There is limited variety in the land use categories, which primarily consists of water bodies, grasslands, and forests, with notable ecological conservation benefits. Areas with average HQ, commonly found in patchy distributions within grasslands and undeveloped areas, are distributed on the Loess Plateau. The YRB's winding bends, southern Shaanxi Province, Shanxi Province, Henan Province, and Shandong Province are the main locations for areas with low to very low HQ. These areas consist mainly of agricultural and construction land. The kind and degree of land use change have an impact on HQ. Forested and

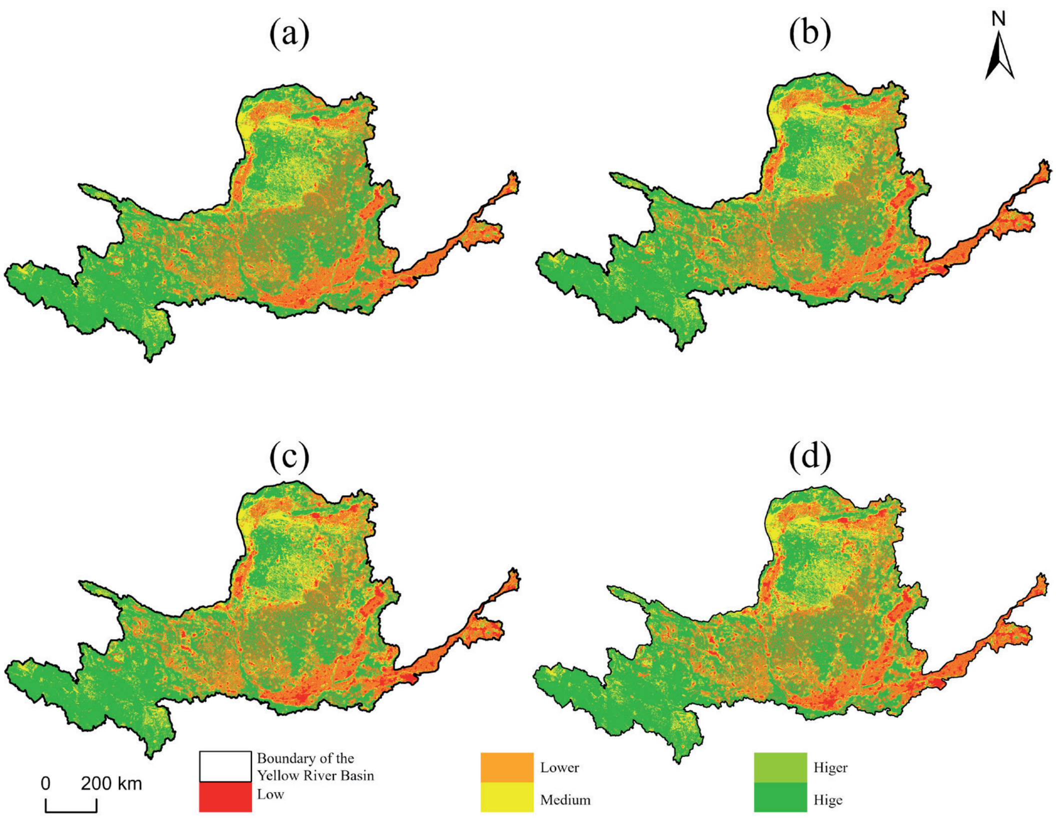

Fig. 4. Spatial Differences in HQ in the YRB from 2008 to 2023. a) HQ in 2008, b) HQ in 2013, c) HQ in 2018, and d) HQ in 2023.

grassland regions help improve HQ, while higher land use intensity leads to lower HQ.

Characteristics of Changes in BCF

Spatio-Temporal Patterns of BCF

Fig. 5 illustrates the NPP quantitative evaluation method analysis of BCF in the YRB from 2008 to 2023.

Overall, from 2008 to 2023, the BCF index of the YRB showed an upward-downward-upward trend, with annual average values increasing sequentially to 0.061, 0.072, 0.073, and 0.079. The boundary between weak and strong conservation functions became increasingly distinct, and the BCF in the basin's lower reaches demonstrated a consistent rising trajectory.

Characteristics of regional variation: The YRB's BCF is distributed spatially in a manner that is "low in the northwest and high in the southeast". Most of the regions with high maintenance function indices are found in central Shandong Province, northwestern Henan Province, southern Shaanxi Province, and southern Shanxi Province. With relatively low elevations (100-1,500 m) and high net primary productivity, these areas benefit from milder temperatures, abundant precipitation, and consequently, more accessible water resources. Most areas with low maintenance function indices are found in southern Gansu Province, all of Ningxia, eastern Qinghai Province, and the southwest portion of Inner Mongolia. These areas are ecologically fragile, with minimal resource availability for organisms due to temperature and precipitation limitations on net primary productivity. For example, eastern Qinghai has lower temperatures and high elevations between 3,500 and 6,100 m. The availability of resources for organisms is impacted by poor net primary productivity and low average monthly precipitation in southern Gansu Province, Ningxia, and southwestern Inner Mongolia.

Changes in BCF Throughout Time and Space

Using ArcGIS 10.8, index difference maps for different periods were generated by subtracting the spatial distribution maps of BCF across years. A difference of one level indicates a minor change, while a difference of two or more levels indicates a significant change. According to Table 3 and Fig. 6, this method divides changes in the watershed's BCF between 2008 and 2023 into five categories: unchanged, slightly reduced, significantly reduced, slightly increased, and significantly increased.

The YRB's BCF has generally improved. The main trend in BCF between 2008 and 2023 was a minor rise, encompassing 62.73% of the region. The Yellow River estuary in Shandong Province, the eastern part of Gansu Province, central and southern Ningxia, central and northern Shaanxi Province, southwestern Shanxi Province, western Henan Province, and the Yellow River headwaters in Qinghai Province were the main locations of this improvement. Significantly improved

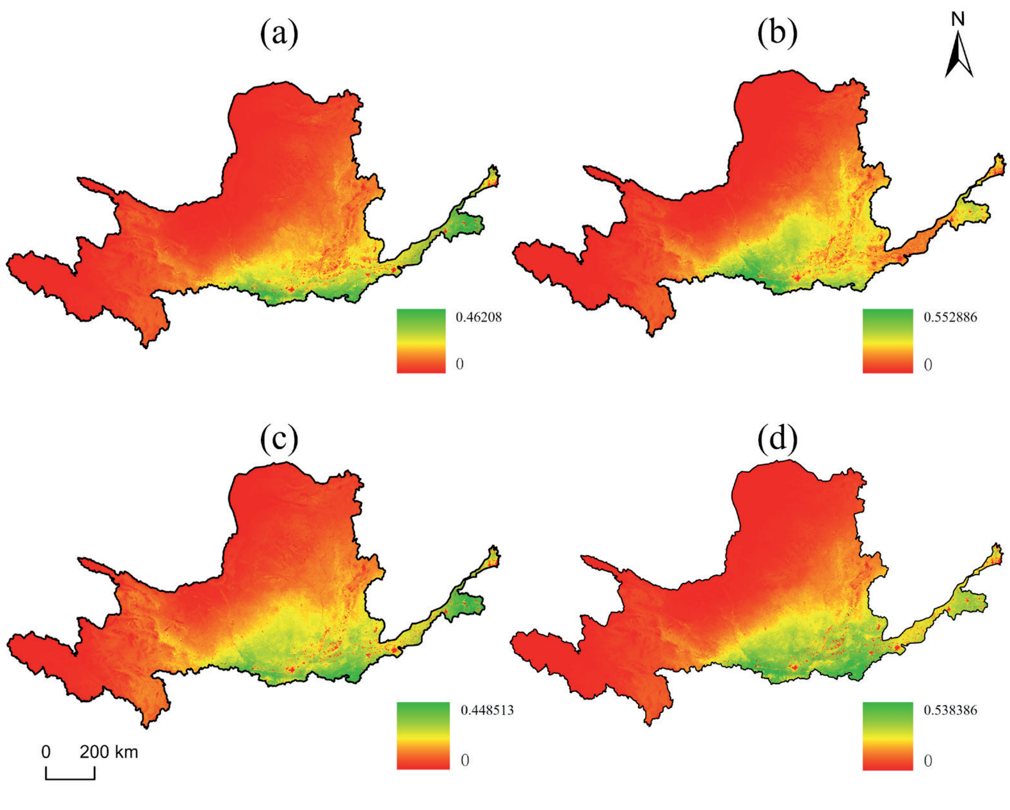

Fig. 5. The YRB's BCF spatial distribution, 2008-2023. a) BCF in 2008, b) BCF in 2013, c) BCF in 2018, and d) BCF in 2023.

Table 3. Variations in the levels of BCF between 2008 and 2023.

Rank Change	2008~2013	2013~2018	2018~2023	2008~2023
Significantly reduced	1.08%	0.20%	0.01%	0.05%
Slightly reduced	19.85%	32.77%	57.98%	25.03%
Unchanged	9.74%	5.28%	7.73%	8.21%
Slightly increased	68.68%	61.10%	33.15%	62.73%
Significantly increased	0.65%	0.65%	1.14%	3.98%

areas made up 3.98% of the total, mostly in the Qin Ling Mountains region near the intersection of the provinces of Shaanxi, Shanxi, and Henan. Areas that had a minor decrease, 25.03%, were mostly found in the Inner Mongolia portion of the Loess Plateau's "U-shaped bend", the junction of Henan and Shandong provinces, and the junction of Qinghai and Gansu provinces. Areas exhibiting a notable decline made up the smallest percentage during the 15-year period.

An analysis by phase reveals that between 2008 and 2013, minor increases predominated, primarily in the Gansu sector of southeast Qinghai Province, parts of Ningxia outside the Ningxia Plain, Shaanxi Province, the Shanxi region, and southeast Inner Mongolia. Regions experiencing minor declines included northeastern Qinghai Province, the Ningxia Plain, northwest Inner Mongolia, the Henan area, and the Shandong section, with the Shandong region in particular experiencing significant declines. Between 2013 and 2018, areas that had previously seen minor declines experienced significant growth, forming a general "sandwich" pattern, while moderate rises remained prevalent, characterized by losses in the center and gains on the sides. In contrast to the previous phase, the subsequent period (2018-2023) saw notable increases in the Ningxia Plain, Henan region, Shandong section, northern Qinghai Province, and northwest Inner Mongolia, alongside modest decreases in Shanxi and Shaanxi. Overall, between 2018 and 2023, the percentage of areas with minor declines was higher than in the preceding two periods. The overall pattern showed modest rises in the southeast and mild declines in the northwest, with 57.98% of the area experiencing slight decreases, including the southwest region of Shandong.

Evolutionary Trajectory of BCF

We investigated the geographical development patterns of BCF in the YRB between 2008 and 2023 using center-of-gravity shift analysis and SDE. As seen in Fig. 7, the results demonstrate notable variations in spatial clustering features throughout the course of the 15-year timeframe.

Throughout the study period, the YRB's overall BCF increased, as seen in Fig. 7. The BCF's SDE in the lower reaches, on the other hand, shows that the ellipticity declined yearly between 2008 and 2013, hitting its lowest point in that year. Between 2013 and 2018, it had

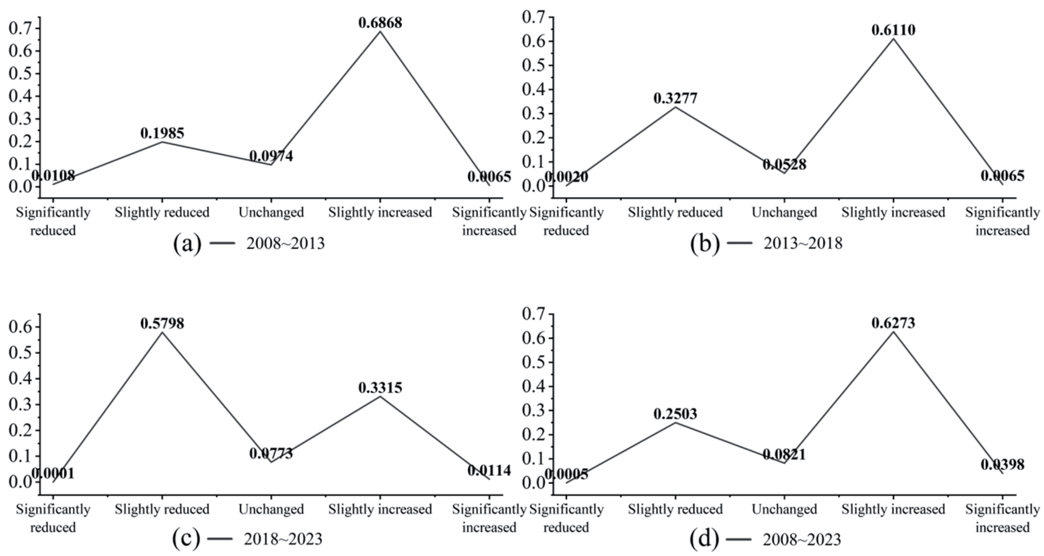

Fig. 6. Variations in the Levels of BCF between 2008 and 2023. a) Variations in the levels of BCF between 2008 and 2013, b) Variations in the levels of BCF between 2013 and 2018, c) Variations in the levels of BCF between 2018 and 2023; (d) Variations in the levels of BCF between 2008 and 2023.

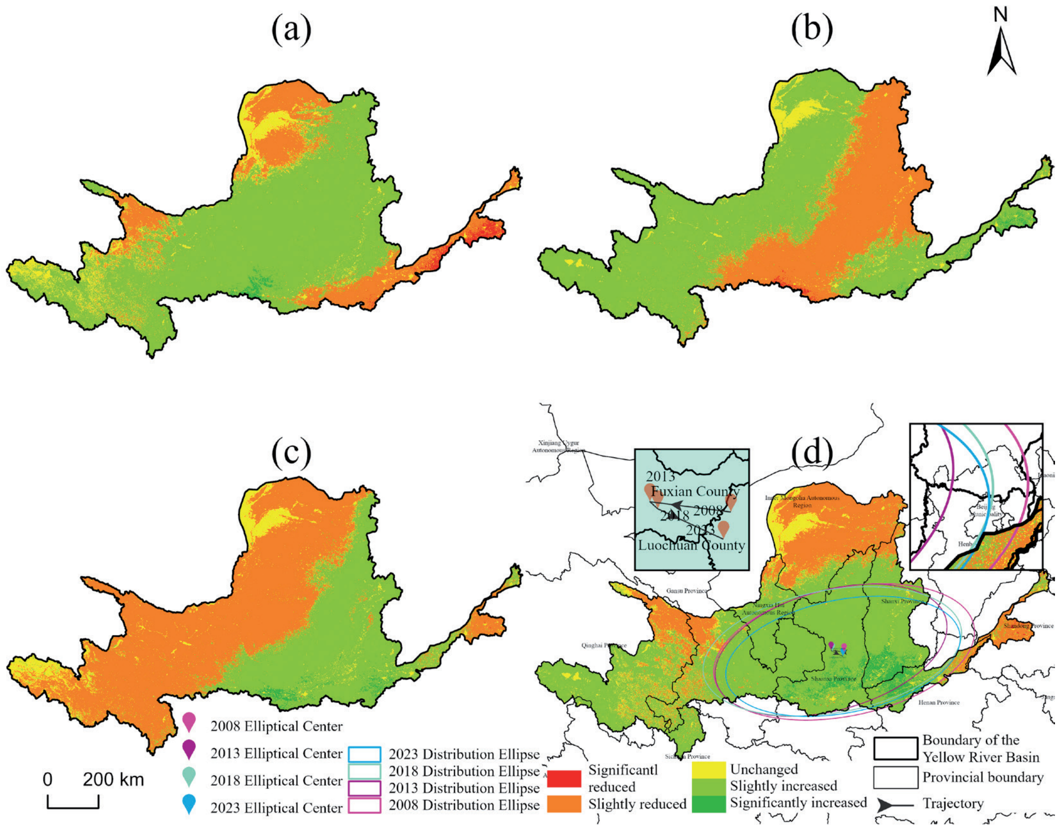

Fig. 7. The Geographical development patterns of BCF in the YRB between 2008 and 2023. a) The geographical changes of BCF in 2008, b) The geographical changes of BCF in 2013, c) The geographical changes of BCF in 2018, and d) The geographical changes of BCF in 2023, as well as the SDE and the center-of-gravity migration model for BCF in the YRB from 2008 to 2023.

a minor recovery. It has since declined yearly because of outside influences like building and land development.

Fig. 8 illustrates how the primary axis's length varied greatly from year to year, showing a pattern of first shortening, then lengthening, and eventually shortening once more. Compared to the major axis, the minor axis's length fluctuated less and generally showed an approximate shrinking trend, but with a significantly lesser amplitude. The major and minor axes' overall trend shows that the elliptical range is progressively getting smaller, with a notable shrinkage from 2008 to 2013 and a steadier pace after that. Additionally, as shown in Fig. 7, the elliptical range varies from year to year, often exhibiting a propensity to migrate southeastward while the overall range continues to shorten. The YRB's BCF hub has been alternating between Shaanxi Province's Luochuan County and Fuxian County. This center has shifted from the top left to the bottom right over the last fifteen years. The distribution of BCF generally exhibits a southwest-to-northeast trend centered on

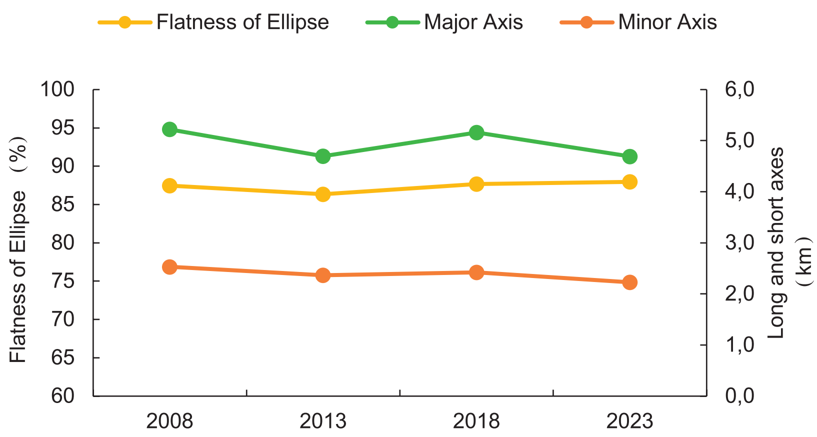

Fig. 8. Analysis of changes in major and minor axes and ellipticity.

Shaanxi Province, suggesting that the conflict between ecological conservation and economic development is still significant in the YRB's middle reaches. Ecological preservation and economic development compete for land use. The overall spatial aggregate of these functions migrated southward and shrunk considerably in comparison to 2008. This spatial shift demonstrates the effectiveness of ecological conservation and governance measures by indicating that the Qinling Mountains and Guanzhong Basin's capacity to conserve biodiversity has steadily increased at a quicker rate than in other areas.

Analysis of the Functional Driving Mechanisms for BCF in the YRB

Contribution of Driving Factors

This study combines economic and resource characteristics with previous research to examine important elements impacting BCF in the YRB [57-59]. Using the XGBoost model and SHAP interpretability analysis, ten driving factors were selected from natural environment and socioeconomic dimensions (Fig. 9). These factors included net primary productivity (X1), annual mean temperature (X2), annual mean precipitation (X3), elevation (X4), slope (X5), Normalized Difference Vegetation Index (NDVI) (X6), HQ (X7), population density (X8), road network density (X9), and Gross Domestic Product (GDP) (X10). The method quantifies the contribution of each variable to the BCF capacity, thereby ensuring the model captures the fundamental interplay between water cycle components, vegetation dynamics, and human pressure.

Based on the SHAP value analysis, the results indicate that among the natural environmental factors, net primary productivity (X1), annual mean temperature (X2), and annual mean precipitation (X3) were the most significant and highest-weighted drivers influencing the BCF. This finding underscores the dominant role of hydro-climatic processes and fundamental components of the regional water and carbon cycles in shaping the capacity for BCF. Subsequently, elevation (X4), GDP (X10), NDVI (X6), and HQ (X7) showed notable contributions, reflecting the important effects of topographic conditions, vegetation vigor, and socioeconomic development. In contrast, variables such as slope (X5), road network density (X9), and population density (X8) had relatively weak impacts on the model output, with their SHAP contribution values mostly concentrated below 0.001, indicating minimal perturbation to the BCF predictions.

Cellular Analysis

According to the SHAP distribution features (Fig. 10), temperature, precipitation, and net primary productivity all show a broad distribution of SHAP values in addition to high contribution values, demonstrating a definite beneficial impact. In other words, increased precipitation, warmer temperatures, and higher net primary productivity all support the conservation of biodiversity.

In low-value zones, GDP has a beneficial impact, but in high-value zones, it has no discernible effect. This suggests that places with lower GDP also have weaker BCF. Positive SHAP values are correlated with high NDVI values, suggesting that regions with a lot of

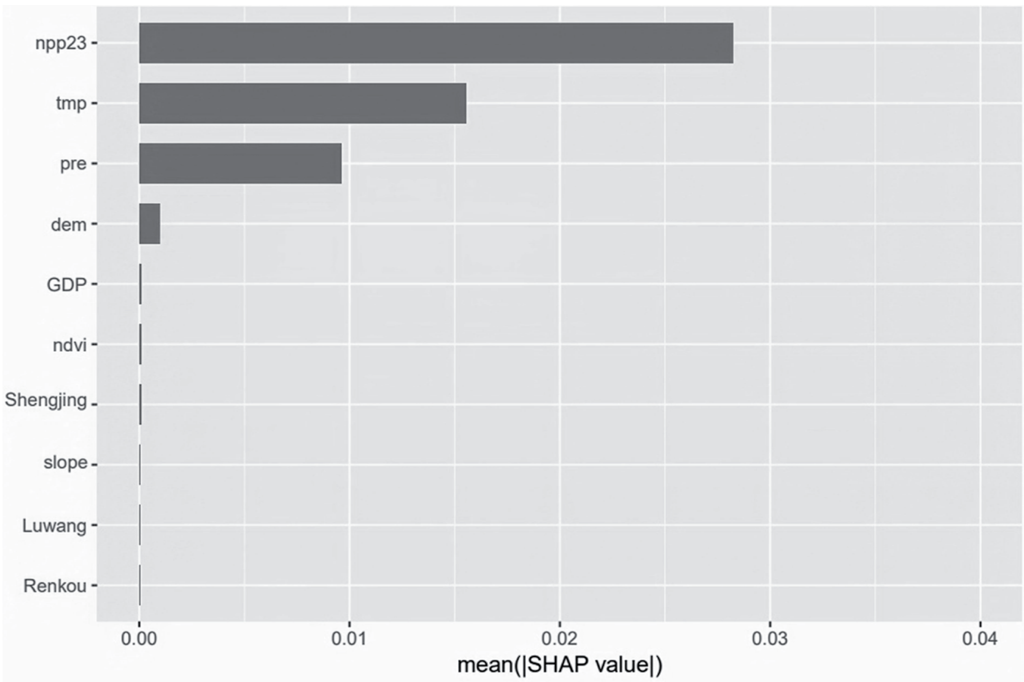

Fig. 9. Ranking of SHAP value contributions for the YRB's principal BCF drivers.

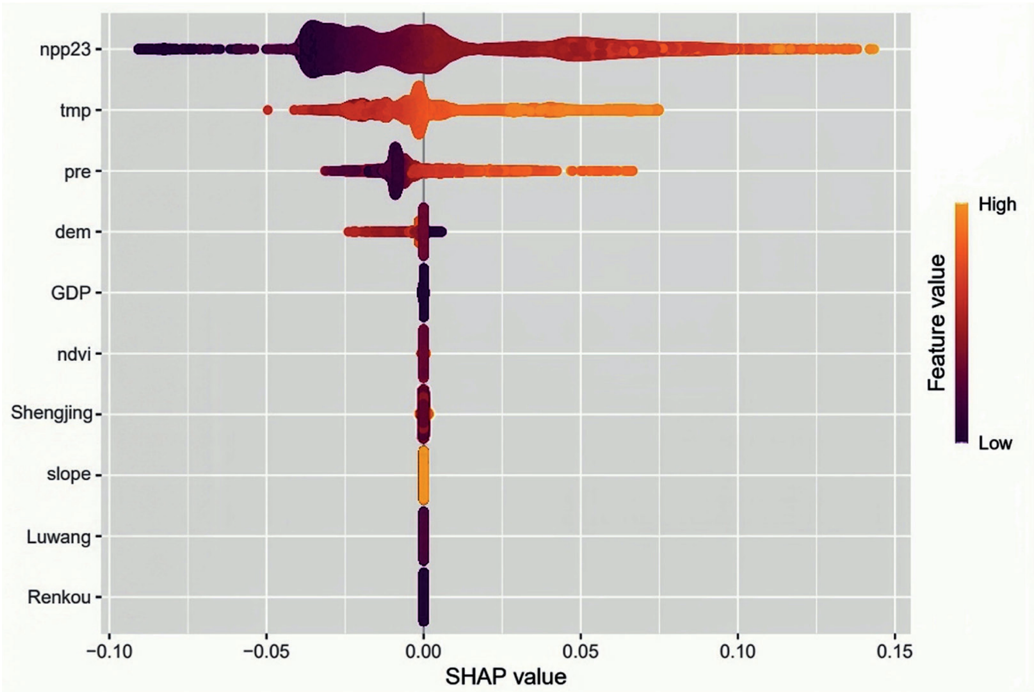

Fig. 10. SHAP distribution of various driving factors affecting BCF in the YRB.

vegetation frequently have stronger BCF. In the zero-value region, HQ parameters exhibit overlapping high and low values, indicating the coexistence of both positive and negative associations. Improving HQ is a prerequisite for increasing biodiversity, as evidenced by the expansion of high HQ values on both positive and negative sides.

In conclusion, the fundamental drivers of BCF are the natural environmental variables of net primary productivity, temperature, and precipitation. Slope and several socioeconomic factors have comparatively little effect. The purpose of this study is to offer quantitative support for the later identification of important protected areas and the optimization of spatial arrangements for the maintenance of biodiversity.

Discussion

The HQ in the YRB remained at a relatively high level (0.68-0.70 on average) but showed a clear "higher in the west, lower in the east" pattern. High-HQ areas were concentrated in the upstream water source regions of Qinghai, dominated by forests and grasslands with critical water conservation functions. Low-HQ areas coincide with intensive agricultural and urban land in the eastern plains, where LUI poses higher risks of non-point source pollution and reduced hydrological connectivity.

In contrast, the BCF showed a distinct "high in the southeast, low in the northwest" spatial disparity, which aligns closely with the basin's precipitation and available water resource gradient. High-BCF areas were identified in the humid Qinling Mountains and Shandong hilly regions, which are essential for freshwater habitat provision. The SDE analysis confirmed this trend, showing the spatial centroid of BCF migrated southeastward toward these more humid areas, while the ellipse's orientation highlighted a southwest-northeast spatial alignment influenced by topography and moisture transport pathways.

The XGBoost-SHAP analysis quantitatively identified net primary productivity (NPP), annual mean temperature, and annual mean precipitation as the three most influential natural drivers (Fig. 9 and Fig. 10). This result underscores that water availability and energy inputs – the core of the regional hydro-climatic system – are the primary determinants of the basin's capacity to provide WRES. Precipitation is the direct source of water, temperature governs evapotranspiration and soil moisture conditions, and NPP reflects the integrated outcome of water and energy use by vegetation. Their combined effect forms the foundational control on the spatial pattern of BCF.

The observed paradox in the middle S-shaped bend, characterized by high HQ but low BCF, can be reinterpreted as a "water-ecological function mismatch". This region, despite having fair vegetation cover (which supports HQ), is likely constrained by limited soil moisture availability, deep groundwater tables, or pronounced seasonal water stress, which restrict the actual water supply to ecosystems. These constraints limit their ability to support complex aquatic communities; a limitation reflected in the low BCF. This finding underscores that in arid and semiarid basins, effective ecological function is not determined by land cover alone but is critically governed by the actual hydrological conditions that regulate water accessibility for ecosystems.

Conclusions

This study demonstrates that the spatial patterns of key WRES (HQ and BCF) in the YRB are fundamentally shaped by hydro-climatic gradients, with precipitation, temperature, and NPP being the dominant drivers. The identified "water-ecological function mismatch" reveals a critical limitation imposed by water scarcity on ecological performance. These findings imply that effective watershed management must transition from a land-centric to a water-centric approach. Ecological conservation and restoration strategies should be guided by the principle of "water-determines-ecology". This involves:

(1) Water conservation and ecological recharge projects should be prioritized in areas with high habitat potential but limited water availability.

(2) Areas where high WRES (both HQ and BCF) overlap must be strictly protected, as they constitute the core of watershed ecological security.

(3) To improve water-related ecosystem monitoring, early warning, and adaptive capabilities and increase "ecological resilience", future initiatives must bolster the use of digital technologies in water resources management and watershed sustainability.

Therefore, moving towards integrated land-water-ecosystem management is imperative. Future strategies should adopt a "water-determines-ecology" principle, prioritizing ecological recharge in water-limited areas with high habitat potential and strictly protecting core zones where high WRES (e.g., water conservation, purification, and biodiversity support) overlap, as these areas are critical for watershed ecological security and sustainable water supply. This work not only provides a novel framework for water resources management and watershed sustainability in arid and semi-arid regions but also offers a replicable model for freshwater ecological conservation applicable to diverse geographical contexts.

Abbreviations

The following abbreviations are used in this manuscript:

YRB	Yellow River Basin
WRES	Water-related ecosystem services
LUI	Land-use intensification
HQ	Habitat Quality
BCF	Biodiversity Conservation Function
InVEST	Integrated Valuation of Ecosystem Services and Trade-offs model
NPP	Net Primary Productivity
SDE	Standard Deviational Ellipse
XGBoost	eXtreme Gradient Boosting
SHAP	Shapley Additive Explanation
GDP	Gross Domestic Product
NDVI	Normalized Difference Vegetation Index

Acknowledgments

We are grateful for the support of the National Social Science Foundation of China and the Ningxia Philosophy and Social Sciences Planning Projects Foundation.

Use of AI Tools Declaration

During the preparation of this work, the author used Google Gemini to improve language clarity, readability, and grammatical accuracy. It was not used to formulate scientific hypotheses, interpret original research findings, or generate raw scientific data. After using this tool, the author(s) reviewed and edited the content as needed and take full responsibility for the content of the published article.

Conflict of Interest

The authors declare no conflict of interest.

Credit Authorship Contribution Statement

Xiao Feng: Conceptualization, Methodology, Resources, Writing – review & editing, Supervision, Project administration, Funding acquisition. Xigan Sun: Conceptualization, Software, Validation, Formal analysis, Investigation, Resources, Data curation, Writing – original draft, Visualization. Huibo Hao: Software, Validation, Formal analysis, Investigation, Resources, Data curation, Visualization.

Funding

This research was funded by the National Social Science Fund of China Project, grant number 21BMZ043. Ningxia Philosophy and Social Sciences Planning Project, grant number 25NXBYJ06.

References

1. JAGO S., BORRELL J.S. Agrobiodiversity conservation enables sustainable and equitable land sparing. Trends in Ecology & Evolution, **39** (10), 877, **2024**.
2. FENG X., WANG L.F., HAO H.B., TIAN X. A Study of Carbon Storage Response and Vulnerability of Land

Use Transformation in Arid Area:taking Ningxia as an Example. Plateau Agriculture, **9** (4), 482, **2025** [In Chinese].
3. LIANG J.L., PAN S.P., XIA N., CHEN W.X., LI M.C. Cross-sensitivity of ecosystem services to land use change in China's poverty-stricken areas. Environmental and Sustainability Indicators, **29**, 101105, **2026**.
4. THEIS S. From local to global: Leveraging localized environmental actions for scalable sustainability effects. PLOS Sustainability and Transformation, **4** (7), e0000185, **2025**.
5. IPBES. Global assessment report on biodiversity and ecosystem services of the Intergovernmental Science-Policy Platform on Biodiversity and Ecosystem Services; BRONDIZIO E.S., SETTELE J., DÍAZ S., NGO H.T., Eds., IPBES secretariat: Bonn, Germany, pp. 1, **2019**.
6. NEWBOLD T., HUDSON L.N., HILL S.L.L., CONTU S., LYSENKO I., SENIOR R.A., BÖRGER L., BENNETT D.J., CHOIMES A., COLLEN B., DAY J., DE PALMA A., DÍAZ S., ECHEVERRIA-LONDOÑO S., EDGAR M.J., FELDMAN A., GARON M., HARRISON M.L.K., ALHUSSEINI T., INGRAM D.J., ITESCU Y., KATTGE J., KEMP V., KIRKPATRICK L., KLEYER M., CORREIA D.L.P., MARTIN C.D., MEIRI S., NOVOSOLOV M., PAN Y., PHILLIPS H.R.P., PURVES D.W., ROBINSON A., SIMPSON J., TUCK S.L., WEIHER E., WHITE H.J., EWERS R.M., MACE G.M., SCHARLEMANN J.P.W., PURVIS A. Global effects of land use on local terrestrial biodiversity. Nature, **520**, 45, **2015**.
7. CEPIC M., BECHTOLD U., WILFING H. Modelling human influences on biodiversity at a global scale – A human ecology perspective. Ecological Modelling, **465**, 109854, **2022**.
8. HILLARD E.M., NIELSEN C.K., GRONINGER J.W. Swamp rabbits as indicators of wildlife habitat quality in bottomland hardwood forest ecosystems. Ecological Indicators, **79**, 47, **2017**.
9. HONG F.T., GUO W.X., WANG H.X. A Comprehensive Assessment of the Hydrological Evolution and Habitat Quality of the Xiangjiang River Basin. Water, **15**, 3626, **2023**.
10. PENG J., PAN Y.J., LIU Y.X., ZHAO H.J., WANG Y.L. Linking ecological degradation risk to identify ecological security patterns in a rapidly urbanizing landscape. Habitat International, **71**, 110, **2018**.
11. LI S.D., WANG X.Z., TAN L., CAI Q.H. Exploring the Drivers Influencing Multidimensional Alpha and Beta Diversity of Macroinvertebrates in Mountain Streams. Water, **16**, 2915, **2024**.
12. HUANG L.N., LI W.B., LIAN Z.M. Loss of biodiversity and its conservation. Journal of Anhui Agricultural Sciences, **37** (5), 2217, **2009** [In Chinese].
13. DUAN H.W., YANG Y.Y., WAN H.W., WANG Y.C., ZHANG Y.S., LU L.H., WAN F.M., DAI Y. Patterns and spatial and temporal dynamics of dynamic habitat indices in Chinese terrestrial ecosystems. Acta Ecologica Sinica, (2), 1, **2025** [In Chinese].
14. XU M.Z., GAO X., WANG H.C. National nature reserve upgrading significantly improves habitat quality: A quasi–natural experiment based on multi–period difference–in–differences model. Natural Resources, **40** (9), 2351, **2025**.
15. YU W.Y., JI R.P., HAN X.Z., CHEN L., FENG R., WU J.W., ZHANG Y.S. Evaluation of the Biodiversity Conservation Function in Liaohe Delta Wetland, Northeastern China. Journal of Meteorological Research, (4), 798, **2020**.
16. LI G.D., FANG C.L., LI Y.J., WANG Z.B., SUN S.W., HE S.W., QI W., BAO C., MA H.T., FAN Y.P., FENG Y.X., LIU X.P. Global impacts of future urban expansion on terrestrial vertebrate diversity. Nature Communications, **13** (1), 1628, **2022**.
17. ZHANG X., LIU Y.S., WANG W., XUE Y.X., LI B.Y., JIN S.Z. Land Use Change in China: A Multi–Scenario Simulation Using the PLUS–InVEST Model and Its Effect on Ecosystem Service Functions. Acta Ecologica Sinica, **45** (19), 9577, **2025** [In Chinese].
18. WU J.Z., PENG X.Y., LIN W.S. Development of forest biodiversity evaluation index system for conifer and broad leaf mixed forest and model construction. Journal of Beijing Forestry University, **37** (4), 8, **2015** [In Chinese].
19. LI W., SUN B.D., CUI L.J., ZHAO X.S., MA Q.F., LEI Y.R., KANG X.M., YU J.J., LIANG Z.R. Evaluation of biodiversity maintenance value of Momog wetland based on double partition dichotomy. Ecological Science, **36** (1), 48, **2017** [In Chinese].
20. JIA L., YU K.X., LI Z.B., LI P., XU G.C., CONG P.J., LI B.B. Spatiotemporal pattern of NPP and its response to climatic factors in the Yangtze River Economic Belt. Ecological Indicators, **162**, 112017, **2024**.
21. PANG B., LI X.X., FU Y. Coupling coordination analysis and obstacle factors of water-energy-environment-economy in the Yellow River Basin. Journal of Cleaner Production, **468**, 143108, **2024**.
22. WANG W., ZHANG Y.Y., TANG Q.H. Impact assessment of climate change and human activities on streamflow signatures in the Yellow River Basin using the Budyko hypothesis and derived differential equation. Journal of Hydrology, **591**, 125460, **2020**.
23. NI Y.X., YU Z.B., LV X.Z., QIN T.L., YAN D.H., ZHANG Q.F., MA L. Spatial difference analysis of the runoff evolution attribution in the Yellow River Basin. Journal of Hydrology, **612**, 128149, **2022**.
24. CHEN G., ZUO D.P., XU Z.X., WANG G.Q., HAN Y.N., PENG D.Z., PANG B., ABBASPOUR K.C., YANG H. Changes in water conservation and possible causes in the Yellow River Basin of China during the recent four decades. Journal of Hydrology, **637**, 131314, **2024**.
25. LI D.Y., FAN Q.Z., GUO D.G. Hydrological effectiveness of ecological governance in the Yellow River Basin: a meta-analysis of water quality and ecosystem responses. Hydrology Research, **56** (10), 1065, **2025**.
26. QIN Z.L., WANG J.X., LU Y. Multifractal Characteristics Analysis Based on Slope Distribution Probability in the Yellow River Basin, China. ISPRS International Journal of Geo-Information, **10** (5), 337, **2021**.
27. MIAO C.H., XIA C., JIN F.J., MA L., ZHANG W.Z., FU B.J. Effectiveness of the implementation of the strategy of ecological protection and high–quality development in the Yellow River Basin and its promotion strategy. Natural Resources, **240** (3), 569, **2025**.
28. ZHANG B.B., CAO J.R., CHEN D.S., LI X., LIU Y.J., WANG J.B., LIU T. Construction of watershed ecological security patterns with integration of spatial variability: A case study of the Yellow River Basin, China. Ecological Indicators, **159**, 111663, **2024**.
29. WEI W., ZHANG Y.L., WEI X.X., XIE B.B., MA Z.Y., LIU C.Y., YU L.N., ZHOU J.J., SHI W., LIU T., LU D. Construction and optimization of ecological security patterns based on ecosystem service function and ecosystem sensitivity in the important ecological functional area–A case study in the Yellow River Basin. Ecological Engineering, **215**, 107609, **2025**.
30. LI J.J., SU P.F., ZHANG J.G. Characteristics and prevention strategies of soil erosion in the ecological

protection and high-quality development planning area of the Yellow River Basin. Bulletin of Soil and Water Conservation, **41** (5), 238, **2021** [In Chinese].
31. ZENG X.J., LI J.C., XIE H.L., ZHU X.H. Impacts of urban expansion process on natural habitat quality in Ganzhou City. Acta Ecologica Sinica, **45** (20), 9881, **2025**.
32. HUANG Z.P., WANG J.D., CHENG Y.F., ZHOU H.H., ZHANG Z., BAO Z.W., YANG C.G. Land use change and future habitat quality assessment in the ecologically fragile area of the middle and lower reaches of the Shule River. Arid Zone Research, (11), 2104, **2025** [In Chinese].
33. ZHOU L., DONG Q.L., PAN Y.J., YANG F., HE M.L., HUANG X., XU J. Spatiotemporal variations and driving forces of regional-scale NPP based on a multi-method integration: a case study in the Beibu Gulf Economic Zone. Ecological Indicators, **174**, 113453, **2025**.
34. POLASKY S., NELSON E., PENNINGTON D., JOHNSON K.A. The impact of land–use change on ecosystem services, biodiversity, and returns to landowners: A case study in the state of Minnesota. Journal of Environmental Management, **48** (2), 219, **2011**.
35. KELEŞ ÖZGENÇ E., UZUN O. Impacts of land use/land cover and climate change on landscape sensitivity in Tunca River sub-basin: Use in spatial planning and sectoral decision processes. Journal of Environmental Management, **363**, 121372, **2024**.
36. ZHANG X.B., LIU Y.N., YIN J.F., SHI P.J., FENG H.Y., SHI J. Multi–scenario simulation of land use change and its impact on ecosystem services in the northeastern edge of the Qinghai–Xizang Plateau, China. Journal of Arid Land, **17**, 145, **2025**.
37. KUNWAR R.M., EVANS A., MAINALI J., ANSARI A.S., RIMAL B., BUSSMANN R.W. Change in forest and vegetation cover influencing distribution and uses of plants in the Kailash Sacred Landscape, Nepal. Environment, Development and Sustainability, **22**, 1397, **2020**.
38. GUO W., TENG Y.J., LI J., YAN Y.G., ZHAO C.W., LI Y.X., LI X. A new assessment framework to forecast land use and carbon storage under different SSP-RCP scenarios in China. Science of The Total Environment, **912**, 169088, **2024**.
39. MOREIRA M., FONSECA C., VERGÍLIO M., CALADO H., GIL A. Spatial assessment of habitat conservation status in a Macaronesian island based on the InVEST model: a case study of Pico Island (Azores, Portugal). Land Use Policy, **78**, 637, **2018**.
40. ANESEYEE A.B., NOSZCZYK T., SOROMESSA T., ELIAS E. The InVEST Habitat Quality Model Associated with Land Use/Cover Changes: A Qualitative Case Study of the Winike Watershed in the Omo–Gibe Basin, Southwest Ethiopia. Remote Sensing, **12** (7), 1103, **2020**.
41. GOLDSTEIN J.H., CALDARONE G., DUARTE T.K., ENNAANAY D., HANNAHS N., MENDOZA G., POLASKY S., WOLNY S., DAILY G.C. Integrating ecosystem–service tradeoffs into land–use decisions. Proceedings of the National Academy of Sciences of the United States of America, **109** (19), 7565, **2012**.
42. WANG K., WANG C., FENG X.M. Research progress on the relationship between biodiversity and ecosystem multifunctionality. Acta Ecologica Sinica, **42** (1), 11, **2022** [In Chinese].
43. YANG J., XIE B.P., ZHANG D.G. Spatial and temporal evolution of habitat quality and its influencing factors in the Yellow River Basin based on InVEST model and GeoDetector. Journal of Desert Research, **41** (4), 12, **2021** [In Chinese].
44. LI X.W., HOU X.Y., SONG Y., SHAN K., ZHU S.Y., YU X.B., MO X.Q. Assessing Changes of Habitat Quality for Shorebirds in Stopover Sites: a Case Study in the Yellow River Delta, China. Wetlands, **39**, 67, **2019**.
45. ZHANG L., ZHENG Y.R. Simulation on the seasonal growth patterns of grassland plant communities in northern China. Chinese Journal of Applied Ecology, (10), 2161, **2008** [In Chinese].
46. LI J.L., CHEN H.L., ZOU C.H., LIU Z.Y., GUO Q.L., GUO P. Vegetation net primary productivity and its temporal-spatial changes in Henan province during 1994-2008. Ecology and Environmental Sciences, **20** (10), 1424, **2011** [In Chinese].
47. MINISTRY OF ECOLOGY AND ENVIRONMENT OF THE PEOPLE'S REPUBLIC OF CHINA, NATIONAL DEVELOPMENT AND REFORM COMMISSION. Guidelines for the Delineation of the Red Line of Ecological Protection; Ministry of Ecology and Environment of the People's Republic of China, National Development and Reform Commission: Beijing, China, **2017** [In Chinese].
48. CHEN H.Y., XIE K.L. NPP-based Importance Evaluation of Biodiversity Maintenance Function in Yunxian County of Yunnan. Shaanxi Forest Science and Technology, **51** (1), 7, **2023** [In Chinese].
49. LI J., LI S., ZHANG Y., PANG J.C. Spatial and temporal changes in biodiversity conservation functions and driver analysis in the Yellow River Basin from 2000 to 2020. China Environmental Science, **43** (9), 4780, **2023** [In Chinese].
50. TANG Y., CHENG Y.P., GAO S., WANG X.Z. Study on the measurement and prediction of the ecological structure for water efficiency in China: from the perspective of "production–living–ecological" function. Environment, Development and Sustainability, **2024**.
51. CHANG X.D., WANG S.J., YANG Z.P., QIN M.Z., MENG X.J., WANG S.Q., LI K. The spatial restructuring process and driving mechanism of China's grain production capacity since the 21st century. Natural Resources, **40** (3), 728, **2025**.
52. YE T.L., ZHANG Y.S. Spatio-temporal Characteristics and Dynamic Evolution of Digital Industry Development in the Beijing-Tianjin-Hebei Region. Social Sciences of Beijing, (1), 15, **2025** [In Chinese].
53. SHENG L.B., RUAN X.M., WANG Y., LV D.Q., CHENG Y. Interpretable XGBoost–SHAP machine learning model for identifying scientific breakthroughs. Scientometrics, **130**, 6801, **2025**.
54. QIU X.L., XIE Y.H., LIANG R.T., ZHU Z.T., ZHOU Y.Q., SUN Y.J. Construction of Cunninghamia lanceolata Crown Width Prediction Model Using Machine Learning for Incremental Learning. Journal of Northeast Forestry University, **53** (12), 48, **2025** [In Chinese].
55. HAN X.Y., YANG Z.H., PENG W., HU Z.H., ZHANG M.T. Effects of machine learning on the simulation of spruce single–timber diameter growth model. Journal of Northeast Forestry University, **53** (10), 46, **2025** [In Chinese].
56. LUNDBERG S.M., ERION G.G., LEE S.I. Consistent Individualized Feature Attribution for Tree Ensembles. arXiv–CS–Machine Learning, (2), 1, **2018**.
57. QIAO Y.J., WANG Z., ZHANG H.N., LIU K., XU W.G. Exploring the Spatially Heterogeneous Relationships Between Biodiversity Maintenance Function and Socio–

Ecological Drivers in Liaoning Province, China. Land, **14** (11), 2276, **2025**.

58. WANG W., WANG H.F., WANG X.Q. Simulation and prediction of the dynamic evolution characteristics of resource– and technology–driven economic development models: a case study of the Yangtze River economic belt in China. Environment, Development and Sustainability, **26**, 17967, **2024**.
59. HE Y., MA S.M., ZHANG L., ZHANG Y.L., HE L.Y. Spatio-temporal change of net primary productivity and the evaluation of the importance of biodiversity maintenance functions in Manas River Basin. Acta Ecologica Sinica, **43** (11), 4664, **2023**.